CHAPTER 7

Evaluation of the Optimal Tubular Adhesive Joint Geometry for Structural Applications

Marcelo M.F.O. ROSAS[1]

Raul D.S.G. CAMPILHO[2]

Raul D.F. MOREIRA[3]

Isidro J. SÁNCHEZ-ARCE[4]

Ricardo J.B. ROCHA[5]

1. INTRODUCTION

Nowadays adhesive bonding technology is present in various industries, such as aeronautics, automotive, marine, wind energy, among others, and can be employed under varied joint geometries and configurations, depending on its application (Ebnesajjad and Landrock 2014). The most frequently used configuration is the single-lap joint due to its simplicity to be manufactured and because the adhesive layer is mainly loaded in shear (O'Mahoney et al.

1 Departamento de Engenharia Mecânica, Instituto Superior de Engenharia do Porto, Instituto Politécnico do Porto, R. Dr. António Bernardino de Almeida, 431, 4200-072 Porto, Portugal.

2 Departamento de Engenharia Mecânica, Instituto Superior de Engenharia do Porto, Instituto Politécnico do Porto, R. Dr. António Bernardino de Almeida, 431, 4200-072 Porto, Portugal. INEGI – Pólo FEUP, Rua Dr. Roberto Frias, 400, 4200-465 Porto, Portugal.

3 INEGI – Pólo FEUP, Rua Dr. Roberto Frias, 400, 4200-465 Porto, Portugal.

4 INEGI – Pólo FEUP, Rua Dr. Roberto Frias, 400, 4200-465 Porto, Portugal.

5 INEGI – Pólo FEUP, Rua Dr. Roberto Frias, 400, 4200-465 Porto, Portugal.

2013). Other joint configurations such as double-lap, stepped-lap or joggle-lap can also be used (Petrie 2000, Machado et al. 2019). In particular cases, it is also feasible to employ butt joints, T-joints, corner joints and tubular adhesive joints (TAJ) configurations (Petrie 2000). In the specific case of the TJA, this type of geometry presents several advantages like larger bonded areas and higher flexural strength due to its overall stiffness (Petrie 2000). Presently, adhesive bonding is widely used in the pipeline industry to perform the connection between pipes (Kaiser and Tan 2020). The earlier methods that were developed in order to predicict the strength of adhesive joints relied on analytical stress analysis (Quispe Rodríguez et al. 2012, de Sousa et al. 2017) and evolved to numerical methods like Finite Element (FE). Currently, the method that is most applied and well-accepted is the Chohesive Zone Models (CZM) (Campilho et al. 2009, Woelke et al. 2013), and with it is possible to accurately simulate bonded joints. The CZM requires previous determination of the adhesive fracture properties. The exactness of the CZM depends on the precise determination of the cohesive strengths, in tension (t_n^0) and shear (t_s^0), and on the fracture toughness, in tension (G_{IC}) and shear (G_{IIC}) (Campilho et al. 2012, Campilho et al. 2013). Athough there are not many studies dedicated to TAJs in the literature, some important works are available (Choi and Lee 1996, Ferreira et al. 2019, Ferreira et al. 2019). In (Albiez et al. 2019) the authors studied experimentally, steel TAJ bonded with two different adhesives (polyurethane and epoxy) and also analyzed the influence of geometrical variations on the joints strength. They settled that the joint strength increases with the increase of the overlap length (L_O), and that no difference is observed between the adhesives. Another remark is that the increase of the adhesive layer thickness (t_A) is prejudical to the joint strength. Nguyen and Kedward (2001) developed an analytical formulation aiming to obtain the shear stress (τ_{xy}) distribution in a TAJ subjet to tension loads. Their analytical formulation was applied to TAJ with aluminium adherends and the results were compared to a FE study with the objective of validating the analytical formulation. The analytical formulation and FE results revealed a good agreement which indicates soundess of the proposed formulation. The authors also concluded that TAJ with a 10° chamfer in the adherends, presented a more uniform stress distribution and a lower value of stress when comparying to joints without chamfering.

In this work it was performed a FE study in combination with CZM to numerically asses the performance of aluminium TAJ loaded under tension and bonded with Araldite® 2015 adhesive. Several geometrical alterations were proposed and analysed to evaluate the strength performance of the joints. In previous works, the numerical model based on CZM considering

axisymmetric elements was compared to experimental results and the model was validated. The selected geometrical alterations analysed in this work were outer chamfer, inner chamfer (both in the adherends), and adding an adhesive fillet at the overlap extremities.

2. MATERIALS AND METHODS

2.1. Materials

The material selected for the tubular adherends was the high strength aluminium alloy AW6082 T651, which was previously characterized (Moreira and Campilho 2015) in bulk tension, which allowed the determination of the following properties: Young's modulus (E) of 70.07±0.83 GPa, tensile yield stress (σ_y) of 261.67±7.65 MPa, tensile failure strength (σ_f) of 324.00±0.16 MPa and tensile failure strain (ε_f) of 21.70±4.24%. For the adhesive it was chosen the moderate ductile adhesive Araldite® 2015 and from the bulk testing (Campilho et al. 2011, Campilho et al. 2013), it was possible to determine E, σ_y, σ_f and ε_f. The shear mechanical properties were determined with Thick Adherend Shear Tests (TAST). For the fracture properties it was used Double-Cantilever Beam (DCB) to determine pure mode I (G_{IC}) and End-Notched Flexure (ENF) tests to determine pure mode II (G_{IIC}) (Campilho et al. 2011, Campilho et al. 2013). The Araldite® 2015 properties are listed in Table1.

Table 1. Mechanical and fracture properties of the adhesive Araldite® 2015 (Campilho et al. 2011, Campilho et al. 2013).

Property	**Araldite® 2015**
Young's modulus, E [GPa]	1.85±0.21
Poisson's ratio, ν	0.33 [a]
Tensile yield stress, σ_y [MPa]	12.63±0.61
Tensile strength, σ_f [MPa]	21.63±1.61
Tensile failure strain, ε_f [%]	4.77±0.15
Shear modulus, G [GPa]	0.70 [b]
Shear yield stress, τ_y [MPa]	14.6±1.3
Shear strength, τ_f [MPa]	17.9±1.8
Shear failure strain, γ_f [%]	43.9±3.4
Toughness in tension, G_{IC} [N/mm]	0.43±0.02
Toughness in shear, G_{IIC} [N/mm]	4.70±0.34

[a] manufacturer's data

[b] estimated from the Hooke's law using E and ν

2.2. Geometry and testing

A schematic representation of the TAJ is shown in Figure 1 and the main dimensions are listed in Table 2. The experimental tests were performed at room temperature in universal testing machine, Shimadzu-Autograph AG-X tester (Shimadzu, Kyoto, Japan) equipped with a 100 kN load cell, and with displacement control of 1 mm/min. Five specimens were tested for each joint configuration and the load-displacement (P-δ) curves were registered for posteriors comparison with the numerical results.

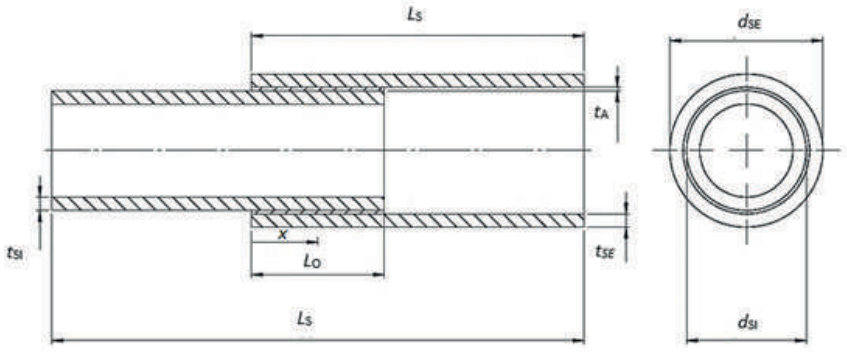

Figure 1. Geometry and characteristic dimensions of the tubular joints.

Table 2. Designation of the dimensions of the specimens and their values (mm)

Designation	**Values [mm]**	
Overlap length, L_O	20	40
Adherends' free length, L_S	50	60
Joint free length, L_T	80	80
Outer diameter of the inner tube, d_{SI}	20,0	20,0
Outer diameter of the outer tube, d_{SE}	22.4	22.4
Thickness of the inner tube, t_{SI}	2	2
Thickness of the outer tube, t_{SE}	2	2
Adhesive thickness, t_A	0.2	0.2

2.3. Numerical modelling

The numerical simulations were perfomed in the FE software Abaqus® and a two-dimensional (2D) axisemetric analysis was considered. Two

models were developed, one for the stress analysis and another for the strength prediction. The aluminium tube adherends were modellled with solid elasto-plastic axisymmetric (CAX4 4-node) elements and the stress-strain (σ-ε) curves were determined (Nunes et al. 2016). For the stress distribution study the adhesive was also modelled with the same solid elements. In the other hand, for the strenght prediciton study the adhesive layer was modelled with one row of axisymmetric cohesive elements that bond the two tubes (COHAX4 4-node). The behaviour of the adheisve layer is mimicked by a contiuunm approcah employing CZM and with mixed-mode softening triangular law shape elements. Only one through-thickness element is consiedered for the adhesive layer that bonds both tubes. More details about this procedure is given in a previous work (Campilho et al. 2011). In order to properly capture the stress profile distribution, it was used models with more refined meshes than the ones for the strength prediction. The element size for the adhesive layer in the models of the stress study (solid elements) was 0.02 mm×0.02 mm and for the strength prediction study (CZM elements) was 0.2 mm×0.2 mm. In Figure 2 is shown a mesh refinement exemple of the TAJ with an overlpap length (L_O) of 20 mm that was used in the strength prediticon study. In terms of boundary condition it was considered that the specimens were clamped at one of the extremeties, and for the loading is applied a longitudinal displacement at the other extremety with transversal restriction.

Figure 2. FE mesh detail and boundary conditions of the axisymmetric model for a tubular joint with L_O=20 mm.

3. RESULTS

3.1. Validation with experimental results

With the goal of validating the numerical maximum load (P_m) results attained by the CZM triangular cohesive softening law, they were compared to experimental ones with two different L_O. The experimental versus numerical results comparison of the strength prediction (P_m) values in function of the L_O for the TAJ bonded with the adhesive Araldite® 2015 are shown in Figure 3. It is possible to observe that the numerical P_m values are in close agreement with the experimental ones. The maximum observed difference between the comparison is 6.1% for the L_O=20 mm and 2.9%

for L_O=40 mm. Since an excellent convergence between the numerical and experimental results was observed, the proposed methodology is considered valid, which will grant soundness to the development of the parametric study carried out in this work.

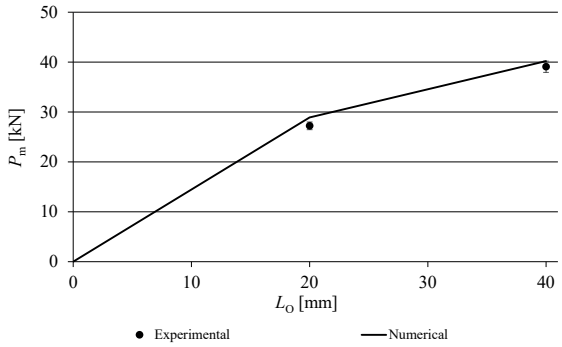

Figure 3. Experimental and numerical values of P_m vs. L_O for the tubular joints with the adhesive Araldite® 2015.

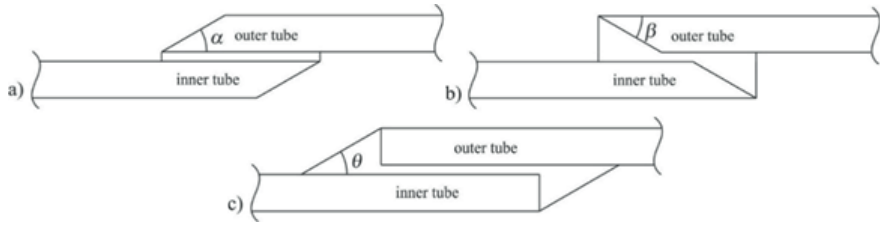

Figure 4. Schematic representation of the outer (a), inner chamfer (b) and adhesive fillet (c) modifications and respective definition of the angles.

3.3. Stress distribution analysis

In this section it will be presented the stress distribution analysis and τ_{avg} is the average value of τ_{xy} for the respective joint.

The first geoemtrical variation analyzed is the outer chamfer angle (α) and the srudied values were: 7,5°, 15°, 30°, 45°, 60° and 90°. It shoulb be emphazised that an angle equal to 90° corresponds to the base case, i.e., adherends without chamfering. In Figure 5 (a) is presented the σ_y/τ_{avg} stress distribution curves, and it is possible to observe peak stresses located at the overlap extremities. The greatest observed decrease on the maximum σ_y/τ_{avg} was 45.6% for α=7.5°, when comparying to the base case(α=90°). The τ_{xy}/τ_{avg} stress distribution is ilustrated in Figure 5 (b) and shows a reduction of

the peak τ_{xy}/τ_{avg} with the decrease of α. It was also observed a 42.7% decrease of the maximum τ_{xy}/τ_{avg} for α=7.5º.

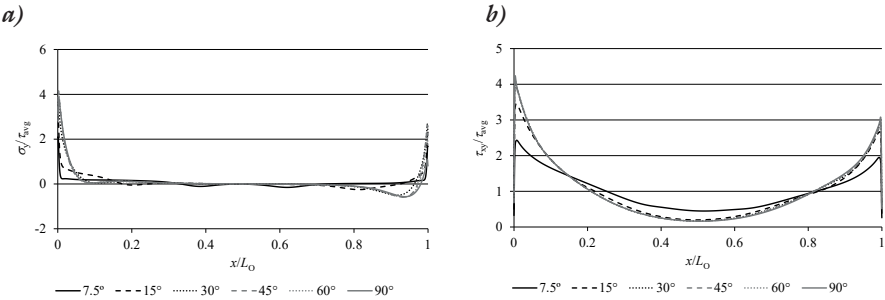

Figure 5. *σ_y (a) and τ_{xy} (b) stress distributions in the adhesive as a function of* α*.*

The stress distribution for the inner chamfer angle (β) is presented in Figure 6. The values assumed for β were 7.5°, 15°, 30°, 45°, 60° and 90°. The σ_y/τ_{avg} stress distribution curves as a function of inner chamfer angle (β) are ilustrated in With the use of inner chamfers at the overlap extremities it can be observed, on the stress profiles, two additional peak stress concentrations, that are added to the already existing ones located at the overlap extremities. The cross section of the chamfered regions was reduced, by the machining process, which gave rise to an increase of the longitudinal strains and consequently led to an increase of the local σ_y/τ_{avg} stress. In contrast the peak stresses located at the overlap extremities were reduced due to the chamfering of the adherends. The inner chamfer results show a reduction of 14.9% for β=30° in the maximum σ_y/τ_{avg} when compared to the base case without chamfer (β=90°). The τ_{xy}/τ_{avg} stress distribution curves are shown in Figure 6 (b). It is also observed two supplementary peak stresses, added to the already existing stress peaks of the overlap extremities. Nevertheless, the difference in this case is more significant, because the intermediate peaks show higher τ_{xy}/τ_{avg} stress values. This indicates that the beginning of the inner chamfer of the TAJ is the most critical zone. In similar way, as the previous analysis, also in this case is observed a reduction of the peak stress τ_{xy}/τ_{avg} with the decrease of β. The maximum obtained reduction was 59.7% for β=7.5º when comparying to β=90º.

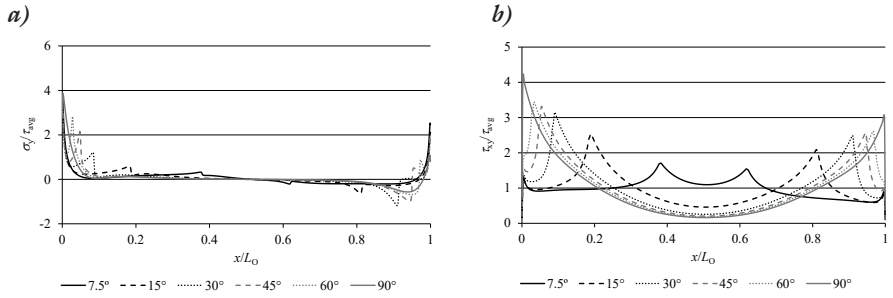

Figure 6. σ_y ***(a) and*** τ_{xy} ***(b) stress distributions in the adhesive as a function of*** β.

Figure 8 shows the stress distribution for the adhesive fillet angle (θ). This geometric varitation causes an increase of L_O and the values of θ analyzed for this case were 7.5°, 15°, 30°, 45°, 60° and 90°. The σ_y/τ_{avg} stress distribution curves depending on θ are presented in Figure 8 (a). The use of adhesive fillet creates additional peak stresses, that appear at $x/L_O<0$ and $x/L_O>1$ in addition to the ones located at $x/L_O=0$ and $x/L_O=1$. Again it is observed an decrease in the the σ_y/τ_{avg} peak stresses with the decrease of θ. The maximum reduction of the peak value (16.7%) is verified for θ=7.5°, when compared to the base case without adhesive fillets (θ=90°). The τ_{xy}/τ_{avg} stress distributions as a function of θ is illustrated in Figure 8 (b) The supplementary peak stresses reveal lower magnitude, when comparying to the ones at the overlap extremities ($x/L_O=0$ and $x/L_O=1$). It was observed a reduction of the peak stresses in the order of 11.7% for θ=7.5°, in comparisson tho the base case (θ=90°), and also a stabilization of peak τ_{xy}/τ_{avg} for the angles ranging between θ=7.5° to θ=60°.

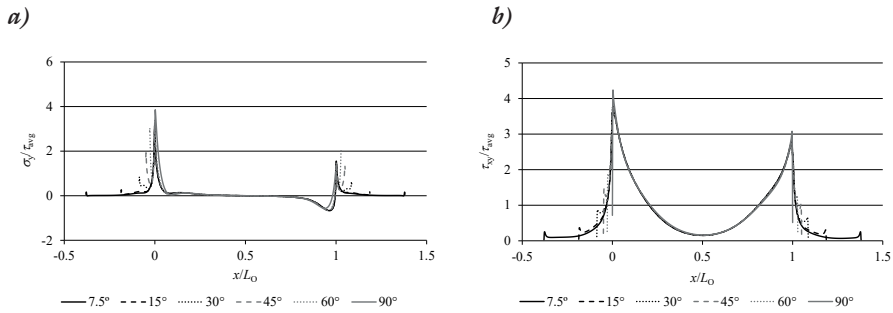

Figure 7. σ_y ***(a) and*** τ_{xy} ***(b) stress distributions in the adhesive as a function of*** θ.

3.4. Strength prediction analysis

The numerical *P*-δ curves for the TAJ bonded with Araldite® 2015 analysed in this work is presented in Figure 8. The strength prediciton for the inner chamfer (Figure 8 (a)) revealed that there is no significant variation of the P_m among the different angles of the outer chamfer. Owing to the overall excellent mechanical properties of this adhesive, plasticitication of the inner tube adherends takes place giving rise to failure dominated by this phenomenon. All numerical P_m values are similar independently of the inner chamfer angle α.

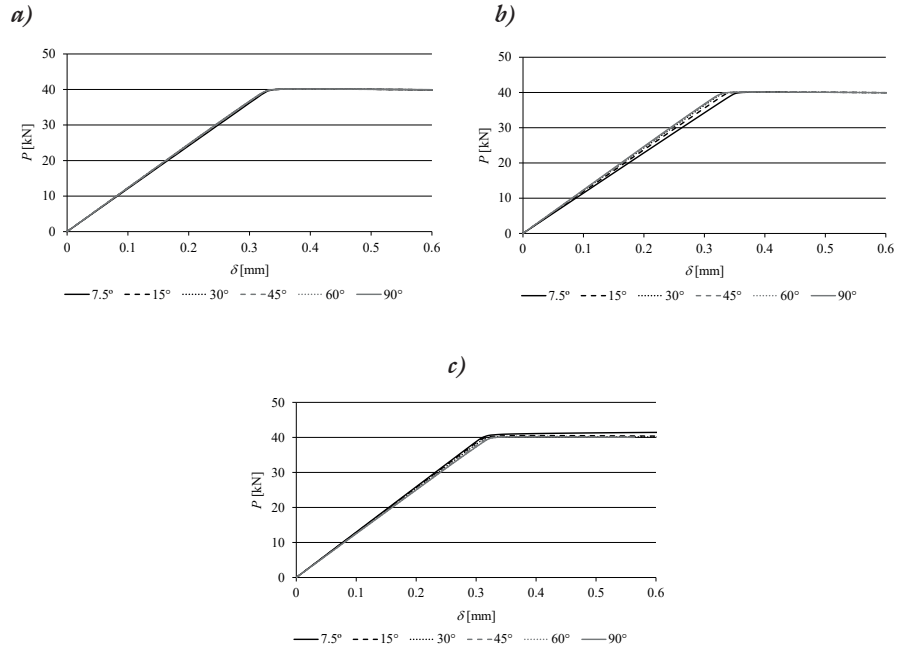

Figure 8. Numerical** P-δ **curves as a function of outer chamfer angle** α **(a), as a function of inner chamfer angle** β **(b), and as a function of ahdeisve fillet angle** θ **(c).

Figure 8 (b) shows the numerical *P*-δ curves for the outter chamfer angle β and is possible to observe that the aluminium tubes undergo plastic deformation in all cases. As a consequence there is a marginal alteration (0.02% for β=30º in comparisson to β=90º) in the P_m with the variation of β. Furthermore, there is a variation in the elastic stiffness of the TAJ with outer chamfers.

The numerical *P*-δ curves for the geometric variation of adhesive fillet θ are given in Figure 8 (c) and in all the cases is possible to detect plasticization of the aluminum adherends. In terms of P_m, it increases while decreasing θ.

The maximum increase obtained is 3.5% for $\theta=7.5^{o}$ in comparisson to the base case without adhesive fillet ($\theta=90^{o}$).

4. CONCLUSION

The tubular adhesive joints strength prediction based on Cohesive Zone Modelling was validated, owing to the numerical maximum strength values being in close agreement to the averaged experimental results. Therefore, the geometrical variations analysed in this work give rise to the following results:

- Outer chamfer (α): for $\alpha=7.5^{o}$ there was a marked σ_y/τ_{avg} and τ_{xy}/τ_{avg} stress decrease in the order of 46%. Regarding the P_m there is no difference between the values of α, since it was observed plastic deformation in the inner aluminium tube;
- Inner chamfer (β): this geometrical variation led to additional stress concentrations peaks. Small σ_y/τ_{avg} stress reductions were obtained ($\approx$15%) and high τ_{xy}/τ_{avg} stress increase were obtained ($\approx$60%). Owing to adherends plasticization there was no marked change in the P_m values;
- Adhesive fillet (θ): The fillet generates supplementary peak stresses at its extremities. With the fillet addition, the overlap peak stresses were reduced approximately 17% for σ_y/τ_{avg} and approximately 12% for τ_{xy}/τ_{avg}. A residual improvement in the P_m (4%) was verified because the shear resistant area increased at the overlap.

In sum it can be settled that the analysed geometric variations can significantly affect the performance of the tubular adhesive joints. Owing to inner tubes plasticization, the pointed out behaviour is not reflected into maximum strength improvements.

REFERENCES

Albiez, M., Vallée, T., Fricke, H. and Ummenhofer, T., 2019. Adhesively bonded steel tubes — Part I: Experimental investigations. International Journal of Adhesion and Adhesives 90, 199-210.

Campilho, R. D. S. G., Banea, M. D., Neto, J. A. B. P. and da Silva, L. F. M., 2012. Modelling of single-lap joints using cohesive zone models: Effect of the cohesive parameters on the output of the simulations. The Journal of Adhesion 88(4-6), 513-533.

Campilho, R. D. S. G., Banea, M. D., Neto, J. A. B. P. and da Silva, L. F. M., 2013. Modelling adhesive joints with cohesive zone models: effect of the

cohesive law shape of the adhesive layer. International Journal of Adhesion and Adhesives 44, 48-56.

Campilho, R. D. S. G., Banea, M. D., Pinto, A. M. G., da Silva, L. F. M. and de Jesus, A. M. P., 2011. Strength prediction of single- and double-lap joints by standard and extended finite element modelling. International Journal of Adhesion and Adhesives 31(5), 363-372.

Campilho, R. D. S. G., de Moura, M. F. S. F., Barreto, A. M. J. P., Morais, J. J. L. and Domingues, J. J. M. S., 2009. Fracture behaviour of damaged wood beams repaired with an adhesively-bonded composite patch. Composites Part A: Applied Science and Manufacturing 40(6–7), 852-859.

Choi, J. H. and Lee, D. G., 1996. An Experimental Study of the Static Torque Capacity of the Adhesively-Bonded Tubular Single Lap Joint. The Journal of Adhesion 55(3-4), 245-260.

de Sousa, C. C. R. G., Campilho, R. D. S. G., Marques, E. A. S., Costa, M. and da Silva, L. F. M., 2017. Overview of different strength prediction techniques for single-lap bonded joints. Proceedings of the Institution of Mechanical Engineers, Part L: Journal of Materials: Design and Applications 231(1-2), 210-223.

Ebnesajjad, S. and Landrock, A. H. (2014). Adhesives technology handbook. New York, USA, William Andrew.

Ferreira, L. R. F., Campilho, R. D. S. G., Barbosa, D. R., Rocha, R. J. B. and Silva, F. J. G., 2019. Static strength improvement of tubular aluminium adhesive joints by the outer chamfering technique. Procedia Manufacturing 38, 629-636.

Ferreira, L. R. F., Campilho, R. D. S. G., Rocha, R. J. B. and Barbosa, D. R., 2019. Geometrical and material optimization of tensile loaded tubular adhesive joints using cohesive zone modelling. The Journal of Adhesion 95(5-7), 425-449.

Kaiser, I. and Tan, K. T., 2020. Damage and strength analysis of Carbon Fiber Reinforced Polymer and Titanium tubular-lap joint using hybrid adhesive design. International Journal of Adhesion and Adhesives 103, 102710.

Machado, R. M. D., Campilho, R. D. S. G. and Rocha, R. J. B., 2019. Extended finite element modelling of aluminium stepped-adhesive joints. The Journal of Adhesion 95(5-7), 450-473.

Moreira, R. D. F. and Campilho, R. D. S. G., 2015. Strength improvement of adhesively-bonded scarf repairs in aluminium structures with external reinforcements. Engineering Structures 101, 99-110.

Nguyen, V. and Kedward, K. T., 2001. Non-linear Modeling of Tubular Adhesive Scarf Joints Loaded in Tension. The Journal of Adhesion 76(3), 265-292.

Nunes, S. L. S., Campilho, R. D. S. G., da Silva, F. J. G., de Sousa, C. C. R. G., Fernandes, T. A. B., Banea, M. D. and da Silva, L. F. M., 2016. Comparative failure assessment of single and double-lap joints with varying adhesive systems. The Journal of Adhesion 92, 610-634.

O'Mahoney, D. C., Katnam, K. B., O'Dowd, N. P., McCarthy, C. T. and Young, T. M., 2013. Taguchi analysis of bonded composite single-lap joints using a combined interface–adhesive damage model. International Journal of Adhesion and Adhesives 40, 168-178.

Petrie, E. M. (2000). Handbook of adhesives and sealants. New York, USA, McGraw-Hill.

Quispe Rodríguez, R., de Paiva, W. P., Sollero, P., Bertoni Rodrigues, M. R. and de Albuquerque, É. L., 2012. Failure criteria for adhesively bonded joints. International Journal of Adhesion and Adhesives 37, 26-36.

Woelke, P. B., Shields, M. D., Abboud, N. N. and Hutchinson, J. W., 2013. Simulations of ductile fracture in an idealized ship grounding scenario using phenomenological damage and cohesive zone models. Computational Materials Science 80, 79-95.